



## Multi-phase Oil Tank Recognition for High Resolution Remote Sensing Images

Changjiang Liu<sup>1</sup>, Xuling Wu<sup>2</sup>, Bing Mo<sup>1</sup> & Yi Zhang<sup>3</sup>

<sup>1</sup>: School of Mathematics and Statistics, Key Lab of Enterprise Informationization and Internet of Things of Sichuan Province, Sichuan Province University Key Laboratory of Bridge Non-destruction Detecting and Engineering Computing, Artificial Intelligence Key Laboratory of Sichuan Province, Sichuan University of Science and Engineering, Zigong, China

<sup>2</sup>: School of Foreign Languages, Sichuan University of Science and Engineering, Zigong, China

<sup>3</sup>: College of Computer Science, Sichuan University, Chengdu, China

### ABSTRACT

With continuing commercialization of remote sensing satellites, the high resolution remote sensing image has been increasingly used in various fields of our life. However, processing technology of high resolution remote sensing images is still a tough problem. How to extract useful information from the massive information in high resolution remote sensing images is significant to the subsequent process. A multi-phase oil tank recognition of remote sensing images, namely coarse detection and artificial neural network (ANN) recognition, is proposed. The experimental results of algorithms presented in this paper show that the proposed processing technology is reliable and effective.

**KEY WORDS:** Artificial neural network, Hough circle transform, Multi-scale retinex with color restoration, Supervised classification

### 1 INTRODUCTION

REMOTE sensing is used in numerous fields, including geography, land surveying and earth science disciplines (Kracker, 1999; Meng, Wang & Cao, 2014; Obade & Lal, 2013; Schnebele & Cervone, 2013). It is also widely used in military, intelligence, commercial, economic, planning, and humanitarian fields (Irvine, Kimball, Regan, & Lepanto, 2014; Cao, Xu & Bian, 2011; Chen & Borcken-Kleefeld). Nowadays, remote sensing generally refers to the use of satellite or aircraft-based sensor technologies to detect and classify objects. Hence, digital image processing and pattern recognition techniques play a great role in solving these problems.

At present, the processing technology of high resolution remote sensing image mainly is divided into two categories; frequency domain and temporal processing (Li, Zang, Zhang, Li & Wu, 2014; Wang, Huo & Feng, 2015). High resolution remote sensing image processing roughly includes five research perspectives; remote sensing image matching, fusion of multi source images and remote sensing image, edge detection of SAR images, remote sensing image classification and remote sensing image change

detection (Zhu, Jiang, Zhou & Addison, 2016). It is critical to classify landmarks from satellite sensors for climate change analysis, urban area studies, forestry applications, risk and damage assessment, water quality assessment, crop monitoring (Jawak, Kulkarni, Luis, 2015; Bruzzone, Demir, 2014). Automatic classification for remote sensing images consists of supervised classification (Stumpf, Lachiche, Malet, Kerle & Puissant, 2014; Xia, Chanussot, Du & He, 2014; Wang, Liu, Xu, Dong and Yang, 2017) and unsupervised classification (Romero, Gatta & Camps-Valls, 2016).

Oil tank, as a high risk object, plays a vital role in the military, environmental protection, and commercial activities. This paper focuses on oil tank recognition from high resolution remote sensing images. Supervised classification is widely used in remote sensing recognition. However, it needs huge samples with a class label. It leads to its limitation in insufficient samples. Beyond that, handling large size remote sensing images is time intensive. Thus, we first analyze characteristics of the oil tank in remote sensing images and device a ROI based detection strategy in combination with shape detection and supervised classification. It is worth noting that target

oil tanks have three distinct properties; homogeneity in luminance, circular shape and texture feature of inside the oil tank. Therefore, we integrated traditional image processing with supervised classification. The homogeneity of luminance makes MSER effective in detecting blobs, which is a rough domain of target oil tank regions. In this paper, output of MSER is used as region of interest or ROI, which reduces the burden of calculation. Prior to circle detection, color and illumination calibration is realized by improved MSRCR. Subsequently, circular shaped regions are extracted by Hough circular transformation, which is thought of oil tank with high probability. We call the aforementioned procedures coarse detection. In fine detection, a high dimensional feature composed of color, texture and shape feature, altogether with class label is applied to ANN.

The remainder of the paper is organized as follows: Multi-phase oil tank recognition is presented in Section 2, including maximally stable extremal regions, multi-scale retinex with color restoration and Hough circular transformation. Experimental results are outlined in Section 3. Finally, we conclude and discuss some directions for future research in Section 4.

## 2 MULTI-PHASE OIL TANK RECOGNITION

IN this paper, a two-phase oil tank recognition in remote sensing images is proposed. It is divided into two steps, in which highly probable oil tank targets are extracted in the first step and final recognition results are obtained by means of high dimensional feature and supervised neural network in the second step. In detail, ROI is determined by MSER algorithm. Then local retinex enhancement on ROI aforementioned is presented. To be followed, circular detection of enhanced local images is implemented. Therefore coarse detection of oil tanks is accomplished by circular detection on the basis of enhanced ROI. We call the above procedures coarse detection. In the second recognition phase, pattern recognition neural network is created on the analysis of color, texture and shape feature. So far, misidentification results are eliminated from coarse detection. Abridged general view of proposed oil tank recognition is shown in Figure 1.

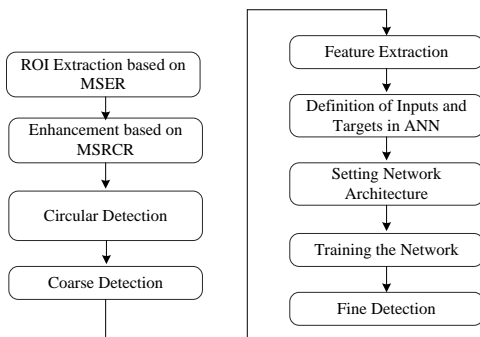


Figure 1. Overview of the Multi-phase Oil Tank Recognition.

### 2.1 Maximally Stable Extremal Regions (ROI setting)

Maximally Stable Extremal Regions, or MSERs are useful algorithm to find out scene elements of interest for gray-scale images, which are used in image matching and recognition (Matas, Chum, Urban & Pajdla, 2004; Chen, Tsai, Schroth, Chen, Grzeszczuk & Girod, 2011; Nistér & Stewénus, 2008). MSERs of the remote sensing image are shown in Figure 2, different blobs painted in various colors. The MSER detection uses a water shedding process to implement as described below.



(a) Remote Sensing Image



(b) MSERs

Figure 2. Remote Sensing Image and MSERs.

The gray-scale image is presented by function:

$$I : \Omega \rightarrow S,$$

Where  $\Omega = [1 \dots W] \times [1 \dots H] \subset Z^2$ ,  $S = [0, \dots, 255]$ .

Maximally Stable Extremal Regions are defined in mathematical form as follows:

1) Connecting relation  $A$ :  $A \subset \Omega \times \Omega$ .

Considering a four-neighbourhood relation, for

$p, q \in \Omega$ , if and only if  $\sum_{i=1}^d |p_i - q_i| \leq 1$ , point

$p$  and  $q$  is connected, and the relation can be denoted by  $p \in A(q)$ , or  $q \in A(p)$ .

- 2) Region D. For any  $p, q \in D \subset \Omega$ , if there exists an ordered sequence  $p, c_1, c_2, \dots, c_n, q$ , such that  $p \in A(c_1), \dots, c_i \in A(c_{i+1}), \dots, c_n \in A(q)$ , D will be called connected subset of  $\Omega$ .
- 3) Boundary  $\partial D$ . It can be presented as:  $\partial D = \{q \in \Omega \setminus D \mid \exists p \in D \text{ s.t. } q \in A(p)\}$ .
- 4) Extremal region D. If  $I(p) > I(q)$  (maximal extremal region) or  $I(p) < I(q)$  (minimal extremal region) always holds for all  $p \in D, q \in \partial D$ .
- 5) Maximally Stable Extremal Regions. Assuming  $D_1, \dots, D_{i-1}, D_i, \dots$  is a sequence of nested external region, namely  $D_i \subset D_{i+1}$ , where  $D_i = \{x \in \Omega \mid I(x) < i, i \in S\}$ . Rate of region change is defined as:

$$r(i) = \frac{|D_i - D_{i-\Delta}|}{|D_{i-\Delta}|}$$

$D_i$  is the MSER, if and only if  $r(i^*)$  is a local minimum. Here,  $|\cdot|$  represents the area of a region,  $\Delta \in S$  is a tiny change of gray level.

Suppose the element of region  $D_i$  assigned white pixel, visualization of  $D_i$  is shown in Figure. 3.

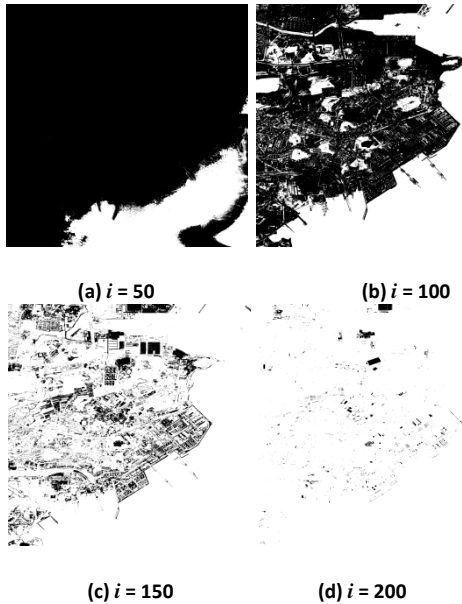


**Figure 3.** Visualization of the  $D_i$  with  $i = 50, 100, 150, 200$ .

As we know, MSERs are shaped in ellipse, whose bounding box is parameterized by the top left corner  $(X_{\min}, Y_{\min})$  and bottom right corner  $(X_{\max}, Y_{\max})$ . Taking a bigger tolerance domain into account, the

bounding box is expanded to the region with the two corners  $(X_{\min} - d_l, Y_{\min} - d_l)$  and  $(X_{\max} + d_l, Y_{\max} + d_l)$ .

## 2.2 Multi-scale Retinex with Color Restoration

Land and McCann (1971) conceived the Retinex theory as a model of the lightness and color perception of human vision. Jobson et al. (1997a) developed a practical implementation of the Retinex theory and defined a single scale Retinex. In the following years, they proposed the multi-scale Retinex with color restoration (MSRCR) (Jobson, Rahman & Woodell, 1997b), which provided not only dynamic range compression with a small scale but also tonal rendition with a large scale.

Multi-scale Retinex (MSR) can be interpreted as:

$$I_i^{MSR}(x, y) = \sum_{n=1}^s \omega_n \frac{\log(I_i(x, y) + 1.0)}{\log(I_i(x, y) + 1.0) * F_n(x, y)}$$

Where  $i = 1, 2, 3$  represents the red, green and blue channel image of  $I$  respectively,  $\omega_n$  is the weight of the  $n$ -th scale of  $s$  scales, and "\*" is convolution operator.

Convolution kernel function  $F_n(x, y)$  is defined as:

$$F_n(x, y) = k_n e^{-\frac{(x+y)^2}{\sigma_n^2}}$$

Where  $\sigma_n$  is the standard deviation of Gaussian function, corresponding to a scale in MSR, the  $F_n(x, y)$  is normalized by the  $k_n$ , such that  $\iint F_n(x, y) dx dy = 1$ .

For the sake of consistency in color, the  $C_i(x, y)$  restoration function is introduced to MSR (Jiang, Woodell and Jobson, 2015):

$$I_i^{MSRCR}(x, y) = C_i(x, y) I_i^{MSR}(x, y)$$

Where  $C_i(x, y)$  is defined as:

$$C_i(x, y) = \log \left( \eta \frac{I_i(x, y) + 1.0}{\sum_{i=1}^3 (I_i(x, y) + 1.0)} \right),$$

Where  $\eta$  is the control parameter.

Normally,  $s = 3$ , or  $\sigma_1 = 5$ ,  $\sigma_2 = 20$ ,  $\sigma_3 = 240$  are used. In previous works (Liu, Cheng, Zhang & Basu, 2017), we proposed an explicit construction method for multiple scales  $s > 3$  as to keep balance in high contrast and color restoration.

### 2.3 Hough Circle Transform

Hough circle transform works in a manner roughly analogous to the Hough line transform (Yuen, Princen, Illingworth & Kittler, 1990; Atherton & Kerbyson, 1999), in which it is parameterized by  $\theta$  (angle) and  $r$  (radius). The approach can be described as;

- 1) Read the remote sensing image  $I$ .
- 2) Convert RGB image to gray scale by eliminating the hue and saturation information while retaining the luminance, denoted the output image by  $G$ .
- 3) Calculate gradient of the  $G$  with the notation  $g_x$ ,  $g_y$  and magnitude  $g = \sqrt{g_x^2 + g_y^2}$ .
- 4) Find indices of the  $g$  whose value is greater than the threshold  $t_e$  and store the  $x$ - and  $y$ -coordinate in the variables  $E_x$  and  $E_y$ .
- 5) Generate a series of equally spaced points between  $R_{\min}$  and  $R_{\max}$ , where  $R_{\min}$ ,  $R_{\max}$  is predefined minimal and maximal radius in application respectively. The sequence can be presented as:

$$R = \{R_{\min}, R_{\min} + d, \dots, R_{\min} + m * d\}.$$

Where  $m = \left\lfloor \frac{R_{\max} - R_{\min}}{d} \right\rfloor$ , the  $d$  usually takes 0.5.

- 6) For any  $r \in R$ , compute the accumulator array as follows:

$$\begin{aligned} x_c &= E_x - R(g_x / g) \\ y_c &= E_y - R(g_y / g) \end{aligned}$$

- 7) Accumulate the votes in the parameter plane, only retain the candidate  $R$ ,  $x_c$  and  $y_c$  whose accumulator is greater than the thresh  $t_a$ .

### 2.4 Artificial Neural Network Recognition (Fine Detection)

In remote sensing images, there are some circular objects, which are actually not oil tanks. The following context will discuss how to eliminate such cases. This phenomenon implies that shape is not the unique characteristics of oil tanks. Multiple trials conclude that high dimension feature vector composed of color, shape and texture can distinguish an oil tank.

#### 2.4.1 Feature Extraction

We consider four categories of feature: Color, texture, shape and HOG. They are defined as:

- 1) Color feature: Denote total number of pixels in the image by  $N$ , the number of pixels with gray level  $l$  by  $n_l$  and the gray levels by  $L$ . Thus the average of the  $k$ -th channel color  $u_k$ , mean

square deviation  $\sigma_k$ , and the entropy  $e_k$  are calculated below:

$$\begin{aligned} u_k &= \frac{1}{N} \sum_{i,j} I_k \\ \sigma_k &= \sqrt{\frac{1}{N} \sum_{i,j} (I_k(i,j) - u_k)^2} \\ p_l &= \frac{n_l}{N}, e_k = -\sum_{l=1}^L p_l \log_2 p_l \\ (l &= 1, 2, \dots, L; k = 1, 2, 3) \end{aligned}$$

- 2) Color histogram: A color histogram of an image is a representation of the distribution of colors. In this paper, HSV color space is chosen, in which the H component (hue) is divided into  $N_h$  bins, S component  $N_s$  bins. Henceforth,  $N_h * N_s$  types of colors are considered. When S component is less than a specific value, human regards as a gray scale, in that case we consider  $N_v$  gray levels. In all, color histogram is  $N_h * N_s + N_v$  dimension. In this paper,  $N_h = N_s = N_v = 10$ , therefore, color feature is 110 dimensional.
- 3) Histogram of oriented gradients (HOG descriptors): Hog descriptors are applied into computer vision and image processing, serving as feature descriptor in object detection. This technique calculates occurrences of gradient orientation in localized parts of an image. In this paper, we divide the entire range of gradient value into 90 bins.
- 4) Invariant moments: M. K. Hu (1962) proposed seven moments, which are translation, scale and rotation invariant. We chose the first 6 Hu moments in this paper.
- 5) Unified local binary pattern: Local binary pattern is a convincing texture descriptor which is widely used in many areas of image processing such as face recognition and defect detection, etc. (Guo, Zhang and Zhang, 2010). Ojala and Harwood (1996) proposed an unified local binary pattern, which simplified local binary pattern to 18 modes.
- 6) Gray level co-occurrence matrix (GLCM): Texture is an image attribute, which describes properties such as smoothness, coarseness, regularity, etc. It shows the organizational structure of the surface and its sequence. Gray level co-occurrence matrix (Haralick, 1973) is a common approach to describe texture by studying the related spatial features of a gray level. Based on GLCM, four indexes such as angular second moments, contrast, correlation and entropy, are also thought of image features.
- 7) Shape feature: The shape of an image is the most important visual feature in image features.

The descriptor of shape feature involves the description of contour boundary, or perimeter and the region within the boundary, or area. In this paper, we employ the width-height ratio and roundness of the minimum area bounding rectangle to describe the shape feature. Assuming the width and height of the bounding rectangle is  $w$  and  $h$  respectively. The width-height ratio is defined as:

$$\alpha = \frac{w}{h}.$$

The roundness is defined as

$$\gamma = \frac{C^2}{A}.$$

Where  $C$ ,  $A$  is the perimeter and area of contouring region respectively.

### 2.4.2 Feed-forward Network to Solve Oil Tank Recognition

We design a two-layer feed-forward network with sigmoid hidden and softmax output neurons to train a neural network, which is able to get rid of the false oil tank objects from the first coarse detection. The network was trained with scaled conjugate gradient back propagation. A 239-150-2 neural network is defined, as shown in Figure 4.

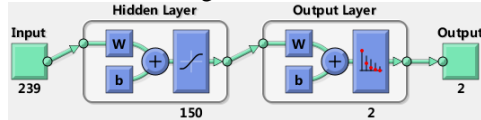


Figure 4. Structure of a Neural Network.

## 3 EXPERIMENTAL RESULTS AND DISCUSSION

WE analyzed dozens of high resolution remote sensing images, containing more than 1000 oil tanks. The algorithm was implemented using the Microsoft Visual Studio development platform supplemented by an Open CV (Computer Vision) library. Experimenting on remote sensing image with the size 2560\*2560, the average execution time (CPU: Intel(R) Core(TM) i5-4210U (2.40 GHz), RAM: 8 GB and OS: Windows 7 (64 bit)) of the proposed algorithm is 1.29 s.

### 3.1 Adaptive Radius $R_{min}$ and $R_{max}$

Ill-suited radius range in Section 2.3 will bring about imperfect detection results, as shown in Figure 5.

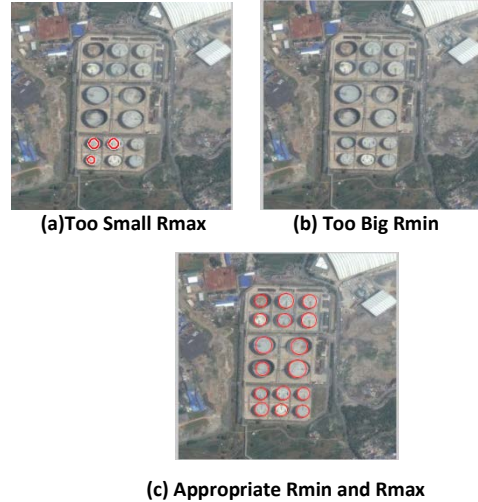


Figure 5. Circle Detection with Various Radius Ranges.

In general, the radius of oil tanks is in the range of 2.65 m-50 m. If spatial resolution is also know, it is easy to calculate the distance in pixel metric. According to this, the radius of experimental remote sensing images in this paper range in [1 21] pel.

### 3.2 MSER

Based on Section 2.1, oil tank regions are extracted by the MSER algorithm, shown in Figure 6(a), in which the union of MSERs bounded by ellipse in green contains all oil tanks. Ellipse shaped MSERs are expanded to rectangular shaped ROIs, as shown in Figure 6(a). Figure 6(c) demonstrates that ROIs extracted only account for 14.7% area of original image. Therefore, it reduces 93% of processing time.

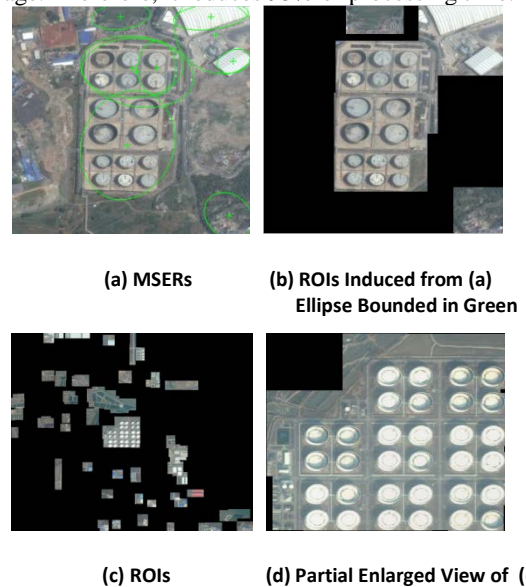


Figure 6. MSERs and ROIs Extracted.

### 3.3 Improved MSRCR based Enhancement

In comparison with the original image, standard MSRCR based enhancement algorithm offer a good contrast, as shown in Figure 7(b). However, it is not hard to find an enhanced image based on the standard MSRCR and cannot retain color consistency. Especially a region rich in texture is excessively smoothed in Figure 7(b). Whereas our method's enhanced image (see Figure 7(c)) performs well in contrast and tonal rendition.

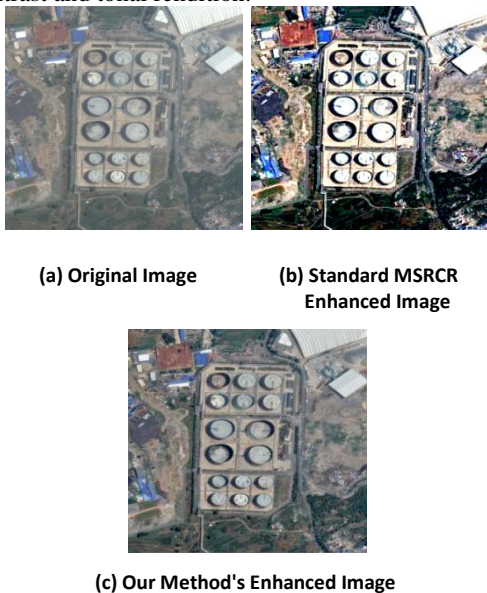


Figure 7. Comparison with the Standard MSRCR.

### 3.4 Artificial Neural Network Recognition

Coarse detection will detect circular objects which is possibly oil tanks. In combination with artificial neural network recognition, namely fine detection, oil tank candidates are to be confirmed. Final detection results are seen in Figure 8 and Figure 9.

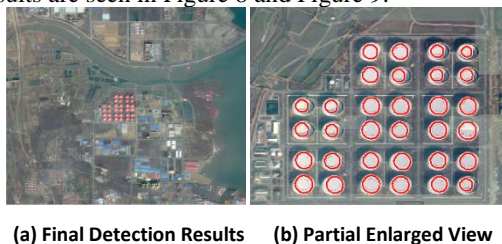


Figure 8. Oil Tank Detection.



Figure 9. Partial Enlarged View of Oil Tanks Recognized by the Proposed Method for Different Remote Sensing Images.

## 4 CONCLUSION

IN this paper, a high-resolution remote sensing image is studied, and a multi-phase oil tank recognition strategy, namely from coarse to fine detection, is proposed. It helps to monitor the environment and prevent crises before they emerge. In this sense, our work significantly improves time performance and rate of identification. In future work, we will conduct experiments on more high resolution remote sensing images, and consider optimizing the algorithm to put it into airborne images. We will also investigate applying more samples to attain high recognition rate and consider accurate localization of oil tanks.

## 5 ACKNOWLEDGMENT

THIS work was supported in part by the Open Project of Key Lab of Enterprise Informationization and Internet of Things of Sichuan Province under Grant No. 2017WZY01, the open Project of the Artificial Intelligence Key Laboratory of Sichuan Province under Grant No. 2014RZY02 and 2017RZJ03, the Open Project of Sichuan Province University Key Laboratory of Bridge Non-destruction Detecting and Engineering Computing under Grant No. 2014QZY01, Natural Science Foundation of Sichuan University of Science and Engineering (SUSE) under Grant No.2015RC08, 2017RCL54 and 2017RCL23, and Educational reform project of SUSE under Grant No. JG-1707. The work was also supported in part by the National Natural Science Foundation of China (Grant No. 11705122) and the Training Programs of Innovation and Entrepreneurship of Sichuan Province for Undergraduates under Grant No.201710622088. The work was also supported in part by Guangxi Key Laboratory of Cryptography and Information Security under Grant No.GCIS201607.

## 6 REFERENCES

- T. J. Atherton and D. J. Kerbyson, (1999). Size invariant circle detection. *Image & Vision Computing*, 17(11), 795-803.
- L. Bruzzone and B. Demir, (2014). *A Review of Modern Approaches to Classification of Remote Sensing Data. Land Use and Land Cover Mapping in Europe.*
- H. Cao, Y. Xu, and Y. Bian, (2011). Sensitivity analysis of region landslide vegetation factor based on the remote sensing and geography information system. *IEEE International Conference on Remote Sensing, Environment and Transportation Engineering*, 4397-4399.
- H. Chen, S. S. Tsai, G. Schroth, D. M. Chen, R. Grzeszczuk, and B. Girod, (2011). Robust text detection in natural images with edge-enhanced Maximally Stable Extremal Regions. *IEEE*

- International Conference on Image Processing*, 2609-2612.
- Y. Chen and J. Borke-Kleefeld, (2014). Real-driving emissions from cars and light commercial vehicles – results from 13 years remote sensing at zurich/ch. *Atmospheric Environment*, 88(5), 157-164.
- V. Dey, Y. Zhang, and M. Zhong, (2014). A review on image segmentation techniques with remote sensing perspective. *Pattern Recognition*, 38(9), 1277-1294.
- Z. Guo, L. Zhang, and D. Zhang, (2010). A completed modeling of local binary pattern operator for texture classification. *IEEE Transactions on Image Processing*, 19(6), 1657-1663.
- R. M. Haralick, (1973). Texture features for image classification. *IEEE Transactions on Systems Man & Cybernetics*, 3(6), 610-621.
- M. K. Hu, (1962). Visual pattern recognition by moment invariants. *Ire transaction of information theory* it-8. *Ire Transactions on Information Theory*, 8(2), 179-187.
- J. M. Irvine, Kimball, J., Regan, and J. A. Lepanto, (2014). Application of commercial remote sensing to issues in human geography. *IEEE Applied Imagery Pattern Recognition Workshop*, 1-11.
- S. D. Jawak, K. Kulkarni, and A. J. Luis, (2015). A review on extraction of lakes from remotely sensed optical satellite data with a special focus on cryospheric lakes. *Advances in Remote Sensing*, 4(3), 196-213.
- B. Jiang, G. A. Woodell, and D. J. Jobson, (2015). Novel multi-scale retinex with color restoration on graphics processing unit. *Journal of Real-Time Image Processing*, 10(2), 239-253.
- D. J. Jobson, Z.-U. Rahman, and G. A. Woodell, (1997a). Properties and performance of a center/surround Retinex. *IEEE Transactions on Image Processing*, 6 (3), 451-462.
- D. J. Jobson, Z.-U. Rahman, and G. A. Woodell, (1997b). A multiscale Retinex for bridging the gap between color images and the human observation of scenes. *IEEE Transactions Image Processing*, 6 (7), 965-976.
- L. M. Kracker, (1999). The geography of fish: the use of remote sensing and spatial analysis tools in fisheries research. *Professional Geographer*, 51(3), 440-450.
- E. H. Land and J. J. McCann, (1971). Lightness and retinex theory. *Journal of the Optical Society of America*, 61(1), 1-11.
- M. Li, S. Zang, B. Zhang, S. Li, and C. Wu, (2014). A review of remote sensing image classification techniques: the role of spatio-contextual information. *European Journal of Remote Sensing*, 47, 389-411.
- C. Liu, I. Cheng, Y. Zhang, and A. Basu, (2017). Enhancement of low visibility aerial images using histogram truncation and an explicit retinex representation for balancing contrast and color consistency. *Isprs Journal of Photogrammetry & Remote Sensing*, 128, 16-26.
- J. Matas, O. Chum, M. Urban, and T. Pajdla, (2004). Robust wide-baseline stereo from maximally stable extremal regions. *Image & Vision Computing*, 22(10), 761-767.
- Q. H. Meng, W. M. Wang, and P. Cao, (2014). Several kinds of remote sensing image's reading and writing and its application in geography national census. *Geomatics & Spatial Information Technology*.
- D. Nistér and H. Stewénius, (2008). Linear time maximally stable extremal regions. *Lecture Notes in Computer Science*, 183-196.
- V. D. P. Obade and R. Lal, (2013). Assessing land cover and soil quality by remote sensing and geographical information systems (gis). *Catena*, 104(5), 77-92.
- T. Ojala and I. Harwood, (1996). A comparative study of texture measures with classification based on feature distributions. *Pattern Recognition*, 29(1), 51-59.
- A. Romero, C. Gatta, and G. Camps-Valls, (2016). Unsupervised deep feature extraction for remote sensing image classification. *IEEE Transactions on Geoscience & Remote Sensing*, 54(3), 1349-1362.
- E. Schnebele and G. Cervone, (2013). Improving remote sensing flood assessment using volunteered geographical data. *Natural Hazards & Earth System Sciences*, 13(3), 669-677.
- A. Stumpf, N. Lachiche, J. P. Malet, N. Kerle, and A. Puissant, (2014). Active learning in the spatial domain for remote sensing image classification. *IEEE Transactions on Geoscience & Remote Sensing*, 52(5), 2492-2507.
- H. Wang, Z. Huo, G. Zhou, L. Wu, and H. Feng, (2015). Monitoring and forecasting winter wheat freeze injury and yield from multi-temporal remotely sensed data. *Intelligent Automation & Soft Computing*, 255-260.
- L. Wang, J. Liu, S. Xu, J. Dong, and Y. Yang, (2017). Forest above ground biomass estimation from remotely sensed imagery in the Mount Tai area using the RBF ANN algorithm. *Intelligent Automation & Soft Computing*, 1-8.
- J. Xia, J. Chanussot, P. Du, and X. He, (2014). (semi-) supervised probabilistic principal component analysis for hyperspectral remote sensing image classification. *IEEE Journal of Selected Topics in Applied Earth Observations & Remote Sensing*, 7(6), 2224-2236.
- H. K. Yuen, J. Princen, J. Illingworth, and J. Kittler, (1990). Comparative study of hough transform methods for circle finding. *Image & Vision Computing*, 8(1), 71-77.
- W. Zhu, H. Jiang, S. Zhou, and M. Addison, (2016). The review of prospect of remote sensing image

processing. *Recent Patents on Computer Science*, 09(999), 53-61.

## 7 DISCLOSURE STATEMENT

NO potential conflict of interest was reported by the authors.

## 8 NOTES OF CONTRIBUTORS



**Changjiang Liu** received Ph.D. degree from Sichuan University, Chengdu, in 2014. He worked as a visiting professor from August 2015 to August 2016 and January 2017 to April 2017 with the Department of Computing Science, University of Alberta, Edmonton, Canada.

He is currently an associate professor with the Sichuan University of Science and Engineering, Zigong, China. His current research interests include image processing and pattern recognition.



**Xuling Wu** received M.S degree from the University of Electronic Science and Technology of China in 2012. She is now working as a lecturer at Sichuan University of Science and Engineering. Her research focused on foreign linguistics and applied

linguistics.



**Bing Mo** received M.E. from Sichuan University of Science and Engineering, Zigong, in 2017. He is currently working as an engineer at Fujian Tietuo Machinery Co., Ltd. His current research interests focused on automation control.



**Yi Zhang** received Ph.D. degree from the National University of Singapore, Singapore, in 2010. He is currently an associate professor with the College of Computer Science, Sichuan University, Sichuan, China. His current research interests focused on image and vision

computing.